frontiers in Plant Science

TYPE Original Research
PUBLISHED 12 March 2026
DOI 10.3389/fpls.2026.1748139



OPEN ACCESS

EDITED BY
Yun Bai,
Hebei Normal University, China

REVIEWED BY
Jingwen Wang,
Chinese Academy of Sciences (CAS), China
Siyu Zheng,
Shenyang Agricultural University, China

*CORRESPONDENCE
Ningbo Cui
cuiningbo@126.com
Xuelian Jiang
jiangxuelian1987@126.com

RECEIVED 03 December 2025
REVISED 29 January 2026
ACCEPTED 06 February 2026
PUBLISHED 12 March 2026

CITATION
Fan M, Wang Z, Jiang X, Cui N, Zhao J, Jiang S, Zhu G, Xing L and Zhang X (2026) Simulation of citrus foliar gas exchange across diverse meteorological conditions: application of the optimal stomatal regulation method. *Front. Plant Sci.* 17:1748139. doi: 10.3389/fpls.2026.1748139



# Simulation of citrus foliar gas exchange across diverse meteorological conditions: application of the optimal stomatal regulation method

Mengying Fan[1], Zhihui Wang[1], Xuelian Jiang[2*], Ningbo Cui[1*], Jingtian Zhao[3], Shouzheng Jiang[1], Guoyu Zhu[1], Liwen Xing[1] and Xiaoxian Zhang[4]

[1]State Key Laboratory of Hydraulics and Mountain River Engineering and College of Water Resource and Hydropower, Sichuan University, Chengdu, Sichuan, China, [2]Key Laboratory of Agricultural Planting Quantization and Application, Weifang University, Weifang, Shandong, China, [3]School of Computer Science and Technology, Algoma University, Sault Ste.Marie, ON, Canada, [4]Sustainable Crops and Soils, Rothamsted Research, Harpenden, United Kingdom

**Introduction:** The optimal stomatal regulation theory provides an eco-evolutionary framework for interpreting the trade-off between $CO_2$ uptake and water loss. This theory postulates that the marginal water cost of carbon gain ($\lambda=\partial E/\partial A$) remains approximately constant over short timescales, thereby offering a mechanistic basis for predicting stomatal behavior and gas exchange.
**Methods:** In this study, leaf-level meteorological variables and gas exchange parameters of orchard citrus were measured throughout the entire phenological period during 2021–2022. We developed a family of optimal stomatal conductance-based models (OSCMs), comprising six forms: Rubisco-limited forms (OSCvc and OSCvcd), RuBP-regeneration-limited forms (OSCvj and OSCvjd), and combined forms that dynamically select the prevailing biochemical limitation (OSC and OSCd).
**Results:** The key parameter $\lambda$ was estimated daily and averaged over the entire phenological period. Using daily $\lambda$ inputs, the three models produced stomatal conductance ($g_s$) with accuracies ranked as OSCvjd ($R^2$ = 0.73) > OSCd (0.63) > OSCvcd (0.40). When a long-term constant $\lambda$ was applied, model performance declined with accuracies ranked as OSCvj (0.66) > OSC (0.52) > OSCvc (0.38).
**Discussion:** The OSC model also produced intercellular $CO_2$ concentration ($c_i$) and photosynthesis ($A$) reasonably well ($R^2$ = 0.78 and 0.48, respectively). Under moderate meteorological conditions (air temperature 30–40 °C and vapor pressure deficit 1–2 kPa), the OSC model showed its best performance with a mean absolute relative error of 35.2% for $g_s$ estimation. Overall, the OSCMs provided a mechanistic approach to simulate citrus leaf gas exchange requiring minimal species-specific traits and routine meteorological inputs. This modeling strategy supports rapid assessment of plant physiological status and estimation of foliar carbon-water fluxes in orchard management under subtropical climates.

KEYWORDS
**citrus, meteorological factors, photosynthetic limitations, stomatal conductance, the optimal stomatal regulation**

# 1 Introduction

Citrus, characterized by millennia-long cultivation history, extensive varietal diversity, distinctive flavors, and high nutritional value, plays an essential role in human diet and agro-processing industry (Palangasinghe et al., 2024). As for 2023, the global citrus planting area has exceeded $8.76\times10^6$ hectares and the annual production has reached $1.35\times10^8$ tons (FAOSTAT, 2025). China contributes nearly 30% of global citrus production, making citrus cultivation a critical component of its agricultural economy, particularly in the hilly regions of Southwest China (Wang et al., 2022). However, regional water scarcity and frequent seasonal droughts have impeded sustainable citrus production (Dong et al., 2024). Such water-related constraints highlight the importance of stomatal regulation in coordinating water loss and carbon assimilation.

Stomata, the primary low-resistance gateway for leaf-atmosphere gas exchange, affect photosynthesis and transpiration directly (Negi et al., 2014). Stomatal function is especially dominant in citrus, where thick cuticles substantially restrict gas diffusion through epidermis (Tominaga and Kawamitsu, 2024). Stomatal aperture can rapidly respond to biotic and abiotic changes, while stomatal anatomy and density adapt more slowly to local climates over evolutionary time (Hetherington and Woodward, 2003). Field studies illustrate pronounced spatiotemporal variability in citrus stomatal behavior: well-managed *Citrus sinensis* L. in South Africa showed seasonal variation with peak stomatal conductance ($g_s$) of 0.14 $mol{\cdot}m^{-2}{\cdot}s^{-1}$ in warm Autumn (Munjonji et al., 2021). In southeastern Brazil, an increase in atmospheric vapor pressure deficit ($D$) from 1.0 to 3.0 kPa reduced $g_s$ by 51% (Souza et al., 2004). On Corsica Island in southern France, the $g_s$ of *Citrus deliciosa* Ten. and *Citrus maxima* Merr. declined by 33–34% during the cold period, whereas the reduction reached 67% in *Citrus medica* L (Santini et al., 2012). Although many studies have investigated citrus stomatal responses, observed patterns differ across regions, climates, and cultivars, highlighting the complexity of stomatal regulation. Therefore, a unified theoretical framework is needed to interpret and predict stomatal behavior across diverse environments.

Researchers have proposed multiple explanations for stomatal behavior. Some argue that stomata respond directly to environmental factors (Jarvis and P., 1976), whereas others suggested that stomatal movement covaries with photosynthesis under given conditions (Ball et al., 1987), and still others emphasized the regulatory role of internal leaf states such as water potential, ion fluxes and cell turgor (Buckley et al., 2003; Delwiche and Cooke, 1977). Amid these diverse perspective, Cowan and Farquhar (1977) proposed a theory of optimal stomatal regulation from an evolutionary and philosophical interpretative angle: an acclimated plant would maximize its carbon gain over a finite water supply, mathematically formulated as maximizing the time integral of $A$-$E/\lambda$. Here, parameter $\lambda$—the marginal water cost of carbon gain ($\partial E/\partial A$)—is typically assumed to be constant over short timescales and adjusted to soil water availability over long timescales (Manzoni et al., 2013). Experimental evidence supporting this framework has been reported for numerous species (Buckley, 2005). However, findings in more complex environments are mixed, prompting further debates on its foundations and applicability. Katul et al. (2010) observed the individual leaf $\lambda$ of *Pinus taeda* L. of North Carolina was steady on short-term but decreased with elevated atmospheric $CO_2$ resulting from prescribed burning. The fluctuations in $\lambda$ with temperature were also observed on *Oryza sativa* L. and *Triticum aestivum* L (Huang et al., 2021). Severe water or heat stress disrupt leaf internal hydraulic and biochemical status, imposing hydraulic failure or non-stomatal limits that violate the optimality assumption (Marchin et al., 2023; Potkay et al., 2025b).

Although uncertainties regarding $\lambda$ variability and model implementation persist, the optimality theory continues to be widely adopted in both empirical and modeling studies (Wang et al., 2020). Finally, two approaches have emerged for applying the optimality theory (Knauer et al., 2018; Manzoni et al., 2011): 1) deriving $\lambda$ analytically from plant gaseous exchange measurements and using its variation to diagnose plant stress; 2) predicting plant gaseous exchange using a prescribed $\lambda$. These two applications constitute the focus of our study, which applies the optimality theory to a citrus orchard in southwestern China and evaluates its applicability.

Directly solving the Lagrange multiplier under optimal hypothesis ($\lambda=\partial E/\partial A$) is inherently challenging (Buckley and Mott, 2013). Some researchers estimate instantaneous $\lambda$ by combining foliar environment variables with gas exchange measurements through physically based or empirical formulations (Medlyn et al., 2013; Volpe et al., 2011). The accuracy of $\lambda$ derived by these approaches depends critically on the quality of input data and the suitability of the computational method employed (Thomas et al., 1999). Beyond gas exchange-based methods, characteristic $\lambda$ values can also be inferred from correlated factors such as vegetation type, soil moisture, plant water potential, and atmospheric $CO_2$ concentration (Lin et al., 2015; Liu et al., 2022; Wang et al., 2019).

From a theoretical perspective, optimal stomatal conductance models provide a mechanistic framework linking carbon assimilation and water loss through the Lagrange multiplier λ, offering a physiologically interpretable basis for predicting gas exchange. By reversing the causal direction in the calculation and prescribing an empirically known $\lambda$ first, gas exchange can be predicted from environmental factors (Mrad et al., 2019). Transforming $\lambda$ into $g_s$ requires gas exchange equations, typically Fick's law of gas diffusion and the Farquhar biochemical model due to their mechanistic basis and minimal empiricism (Medlyn et al., 2011). These coupled optimal stomatal conductance-based models (OSCMs) can simultaneously solve for stomatal conductance ($g_s$), photosynthesis ($A$), transpiration ($E$) and intercellular $CO_2$ concentration ($c_i$) using species traits and atmospheric inputs without cumbersome calibration work. Within this framework, plant gas exchange variables are often predicted with high fidelity (Buckley and Mott, 2013). Ji et al. (2017) predicted the $g_s$ of well-watered soybean and maize with $R^2$ value of 0.86 and 0.88, respectively. Lu et al. (2016) successfully captured the responses of $A$, $E$ and water use efficiency (*WUE*) along rainfall gradients across diverse forest sites.

In addition, two uncertainties arise in the application of the OSCMs. First, as research on stomatal behavior advances, evidence suggest that using hydraulic structural risks rather than transpiration water loss may more accurately represent the water

cost for plants (Dewar et al., 2018; Wolf et al., 2016). Accordingly, the assumption of a constant Lagrange multiplier $\lambda$ should be applied with caution, especially in arid regions (Potkay et al., 2025a; Venturas et al., 2018). Second, within the sub-equation of the OSCMs, the Farquhar functions adopt two different forms depending on photosynthetic limitations: either the $CO_2$ carboxylation rate (Rubisco) or the electron transport rate (RuBP) (Vico et al., 2013). Some studies have preferred to assume a single dominant limitation to achieve a neat analytical expression and smooth solutions (Katul et al., 2010; Schymanski et al., 2015). However, in natural environments, limitations may shift due to fluctuations in water availability, light, temperature, and various other abiotic factors (Abdulbaki et al., 2022; Perdomo et al., 2017).

In this study, two years of citrus leaf gas exchange data were collected from a citrus orchard in southwestern China. Analytical $\lambda$ under diverse meteorological conditions were examined and the applicability of the conventional optimal stomatal model was discussed. Our objectives were to: 1) calculate the marginal water cost of carbon gain $\lambda$ and determine its characteristic values for citrus; 2) modify the optimal stomatal conductance-based models (OSCMs) by distinguishing Rubisco and RuBP scenarios, acknowledging that photosynthetic limitations may vary under different environmental conditions, and predict citrus gas exchange; 3) analyze the main factors affecting model performance and recommend suitable environmental conditions for its application. This research aims to enhance understanding of citrus foliar gas exchange and stomatal regulation in seasonal arid regions and provide a low-input method for forecasting agricultural water-carbon fluxes.

# 2 Materials and methods

## 2.1 Experimental site

The measurements were conducted on six-year-old citrus (*Citrus Tachibana* Tanaka.) grafted onto tangerine rootstock (*Citrus Reticulata* Blanco.) during the phenological period (March–November) in an artificial citrus orchard in Qionglai city, Sichuan province, China (103.45°E, 30.34°N). The citrus orchard is situated at an altitude of 547 m in a subtropical monsoon climate zone characterized by abundant but seasonally uneven rainfall and solar radiation. The multi-year averages of air temperature, relative humidity, and annual precipitation were 16.8 °C, 82%, and 1041.3 mm, respectively. During the two experimental years, the mean air temperature, humidity, solar radiation, and annual precipitation were 17.6 °C, 93.2%, 10.2 $MJ{\cdot}m^{-2}{\cdot}day^{-1}$, and 1013.7 mm, respectively (Figure 1).

The experimental aerated greenhouse was located in a shallow hilly zone, with an average soil bulk density of 1.13 $g{\cdot}cm^{-3}$ and a maximum water-holding capacity ($\theta_f$) of 35.4% volume moisture content. Soil moisture was maintained at 60–75% $\theta_f$ through irrigation, with total irrigation amounts of 347.56 and 313.48 mm in 2021 and 2022, respectively. Fertilization during the entire phenological period totaled 1167 $kg{\cdot}hm^{-2}$, with a nutrient composition of 19-19-19 ($N\text{-}P_2O_5\text{-}K_2O$) percent by weight. According to conventional management, the proportions of basal fertilizer and topdressing applied during the shooting, fruit setting, and fruit expanding stages were 2:1:3:4. Citrus trees were planted at a spacing of 4 m × 3 m. Vigorous citrus trees of similar growth, with height of 2.3–2.5 m, were selected for observation.

## 2.2 Measurement

### 2.2.1 Measurements of leaf gas exchange

Fully expanded citrus leaves on secondary shoots of similar sizes were selected for photosynthetic gas exchange measurements. For each tree, 4–6 leaves from two opposite orientations were tested without strictly distinguishing between sunlit and shaded positions (Figure 2). Gas exchange measurements were conducted as instantaneous observations on multiple leaves sampled at different times of the day; on full-day measurements, leaves measured in the morning were re-measured in the afternoon. Measurements were performed on rain-free days from April to October using infrared gas analysis systems (LI-6400XT, LI-COR Inc., Arizona, USA; Lcpro-SD, ADC Ltd., Hertfordshire, UK). At the start of each measurement day, the instrument was preheated for 30 minutes to routine check, including verifying the seal integrity of the leaf chamber and gas path, ensuring chemical effectiveness, and eliminating analyzer zero offset to guarantee data reliability. After validation, the selected functional leaves were tested *in situ* under ambient light conditions. A total of 1001 and 851 leaf gas exchange datasets were collected in 2021 and 2022, respectively (Table 1).

### 2.2.2 Measurements of leaf net photosynthesis-$CO_2$ response ($A$-$c_i$) curve

On 22$^{nd}$ April and 20$^{th}$ October 2022, the response of functional leaves to varying $CO_2$ concentrations were measured using a LI-6400XT system equipped with RGB red-blue light sources and a $CO_2$ injection device. Prior to measurements, an eight-point calibration was performed to minimize the influence of ambient air fluctuations. Leaves were first acclimated for 30 min at a photosynthetically active radiation of 1000 $\mu mol{\cdot}m^{-2}{\cdot}s^{-1}$ and a $CO_2$ concentration of 400 $\mu mol{\cdot}mol^{-1}$ until gas exchange parameters stabilized. Subsequently, $CO_2$ concentrations in the cuvette were adjusted stepwise, and measurements at each level were recorded after stabilization or after a maximum of 5 min. The $CO_2$ sequence was set as follows: 400, 300, 200, 150, 100, 50, 400, 400, 600, 800, 1000, 1200, 1500, 1800, and 2000 $\mu mol{\cdot}CO_2{\cdot}mol^{-1}$. During the curve measurements, temperature and humidity were not actively controlled to conserve battery power. However, both variables remained relatively stable throughout each test, and the resulting uncertainties were considered acceptable.

## 2.3 Parameter acquisition and model development

### 2.3.1 Calculation of photosynthetic characteristic parameters

The parameters including $K_m$, $\Gamma^*$, $V_{cmax25}$, $J_{max25}$, and $R_{d25}$ were fitted from $A$-$c_i$ curves based on the photosynthetic biochemical

10.3389/fpls.2026.1748139

FvCB model and were assumed to be either constant or temperature-dependent, representing the photosynthetic traits of the studied citrus species. Under natural conditions, photosynthetic TPU limitation is rarely reached, rapidly transitioning to Rubisco-limited or RuBP-regeneration-limited states (Duursma, 2015; Rogers et al., 2021). Therefore, only the Rubisco and RuBP limitations were considered in this study. The FvCB model are shown in Equations 1–3 (Farquhar et al., 1980; Sharkey, 1985):

$$A = \min\{w_c,\ w_J\}\left(1 - \frac{\Gamma^*}{c_c}\right) - R_d \tag{1}$$

$$w_c = \frac{V_{cmax} \cdot c_c}{c_c + K_m},\ K_m = K_c\left(1 + \frac{O}{K_o}\right) \tag{2}$$

$$w_J = \frac{J \cdot c_c}{4c_c + 8\Gamma^*},\ J = \frac{\alpha \cdot Q}{\left(1 + \frac{\alpha^2 Q^2}{J_{max}^2}\right)^{0.5}} \tag{3}$$

Where $A$ is the net photosynthetic rate, μmol·m$^{-2}$·s$^{-1}$; $w_c$ and $w_J$ are the limited carboxylation rate by Rubisco and RuBP, respectively, μmol·m$^{-2}$·s$^{-1}$; $\Gamma^*$ is the $CO_2$ compensation concentration at chloroplast thylakoids, μmol·mol$^{-1}$; $R_d$ is the rate of mitochondrial respiration under light, μmol·m$^{-2}$·s$^{-1}$; $V_{cmax}$ is the maximum rate of Rubisco carboxylation activity, μmol·m$^{-2}$·s$^{-1}$; $K_c$ and $K_o$ are the Michaelis Menten coefficients of Rubisco activity for $CO_2$ and $O_2$, respectively; $O$ is the intercellular $O_2$ concentration, mmol·mol$^{-1}$; $J$ is the rate of electron transport, μmol·m$^{-2}$·s$^{-1}$; $J_{max}$ is the potential maximum rate of electron transport, μmol·m$^{-2}$·s$^{-1}$; $Q$ is the photosynthetic photon flux density, μmol·m$^{-2}$·s$^{-1}$; $\alpha$ is the quantum yield of electron transport, dimensionless; $c_c$ is the $CO_2$ concentration in the carboxylation site of chloroplast thylakoids, μmol·mol$^{-1}$.

Parameters $V_{cmax}$ and $J_{max}$ are temperature-dependent and can be estimated from $A$-$c_i$ curves, then normalized to 25°C using Equation 4 (Medlyn et al., 2002):

$$f(T_k) = k_{25}\exp\left[\frac{E_a(T_k - 298)}{(298RT_k)}\right]\frac{1 + \exp\left(\frac{298\Delta S - H_d}{298R}\right)}{1 + \exp\left(\frac{T_k\Delta S - H_d}{T_kR}\right)} \tag{4}$$

Where $T_k$ is leaf kelvin temperature, K; $R$ is the gas constant, J·mol$^{-1}$·K$^{-1}$; $k_{25}$ is the biochemical parameters including $V_{cmax25}$ and $J_{max25}$, μmol·m$^{-2}$·s$^{-1}$; $\Delta S$ is entropy term, J·mol$^{-1}$·K$^{-1}$; $E_a$ is the rate of exponential increase of the biochemical parameters below the optimum temperature, J·mol$^{-1}$; $H_d$ is the rate of decrease of the biochemical parameters above the optimum temperature, J·mol$^{-1}$. The detailed values of $\Delta S$, $E_a$, and $H_d$ for $V_{cmax25}$ and $J_{max25}$ are shown in Table 2.

Parameters $\Gamma^*$, $K_c$, and $K_o$ also depend on temperature, calculated by Equations 5–7:

$$\Gamma^* = 42.75\exp\left[\frac{37830(T_k - 298)}{(298RT_k)}\right] \tag{5}$$

$$K_c = 274.6\exp\left[\frac{80500(T_k - 298)}{(298RT_k)}\right] \tag{6}$$

$$K_o = 419.8\exp\left[\frac{14500(T_k - 298)}{(298RT_k)}\right] \tag{7}$$

Assuming the mesophyll conductance ($g_m$) approaches infinity, the $CO_2$ concentration at the carboxylation site ($c_c$) can be

TABLE 1 Summary of leaf gas exchange measurement dates and environmental conditions.

| Order | Date (yyyy-mm-dd) | Time | Measure | Weather | Average soil moisture (%) |
|---|---|---|---|---|---|
| 1 | 2021-04-29 | 9:00-17:00 | 325 | sunny | 26.49 |
| 2 | 2021-06-29 | 9:30-12:00 | 80 | overcast | 26.60 |
| 3 | 2021-07-02 | 10:00-18:00 | 141 | cloudy | 24.45 |
| 4 | 2021-07-03 | 10:00-18:00 | 115 | overcast | 22.66 |
| 5 | 2021-07-20 | 10:00-17:00 | 67 | overcast | 21.66 |
| 6 | 2021-07-31 | 9:00-17:30 | 113 | sunny | 26.75 |
| 7 | 2021-08-02 | 9:30-10:30 | 37 | cloudy | 26.06 |
| 8 | 2021-08-06 | 9:30-10:30 | 37 | sunny | 24.09 |
| 9 | 2021-09-15 | 9:00-12:00 | 86 | cloudy | 24.43 |
| 10 | 2022-04-29 | 9:00-12:00 | 26 | cloudy | 23.62 |
| 11 | 2022-06-24 | 9:00-12:00 | 28 | cloudy | 26.70 |
| 12 | 2022-07-06 | 9:00-16:00 | 302 | overcast | – |
| 13 | 2022-07-07 | 9:00-12:00 | 226 | overcast | – |
| 14 | 2022-07-21 | 9:00-12:00 | 86 | overcast | 26.80 |
| 15 | 2022-07-22 | 10:00-13:00 | 76 | overcast | 26.80 |
| 16 | 2022-08-09 | 9:00-11:30 | 26 | cloudy | 22.58 |
| 17 | 2022-10-01 | 10:00-10:30 | 81 | cloudy | 26.83 |
| sum | | | 1852 | | |

10.3389/fpls.2026.1748139

TABLE 2 List of symbol descriptions, units, source and default parameter values used in model calculations.

| Symbol | Descriptions | Units | Source | Value |
|---|---|---|---|---|
| $A$ | net photosynthetic rate | μmol·m-2·s-1 | meas | |
| $E$ | transpiration rate | mmol·m-2·s-1 | meas | |
| $g_s$ | stomatal conductance to water | mol·m-2·s-1 | meas | |
| $c_i$ | intercellular CO2 concentration | μmol·mol-1 | meas | |
| $Q$ | photosynthetic photon flux density | μmol·m-2·s-1 | meas | |
| $T_a$ | Leaf surface air temperature | °C | meas | |
| $T_l$ | leaf temperature | °C | | $T_a$ |
| $T_k$ | leaf kelvin temperature | K | | $T_l$ + 273.15 |
| $D$ | vapor pressure deficit | kPa | meas | |
| $c_a$ | ambient CO2 concentration | μmol·mol-1 | meas | |
| $P$ | air pressure of the atmosphere on leaf surface | kPa | meas | |
| $w_c$ | limited carboxylation rate by Rubisco | μmol·m-2·s-1 | Eq. 2 | |
| $w_j$ | limited carboxylation rate by RuBP | μmol·m-2·s-1 | Eq. 3 | |
| $\Gamma^*$ | CO2 compensation concentration at chloroplast thylakoids | μmol·mol-1 | Eq. 5 | |
| $R_d$ | mitochondrial respiration rate under light | μmol·m$^{-2}$·s$^{-1}$ | Eq. 4 | |
| $R_{d25}$ | mitochondrial respiration rate under light at 25°C | μmol·m$^{-2}$·s$^{-1}$ | cali | 1.77 |
| $V_{cmax}$ | maximum rate of Rubisco carboxylation activity | μmol·m$^{-2}$·s$^{-1}$ | Eq. 4 | |
| $V_{cmax25}$ | maximum rate of Rubisco carboxylation activity at 25°C | μmol·m$^{-2}$·s$^{-1}$ | cali | 43.21 |
| $K_m$ | Michaelis Menten coefficients of Rubisco activity | μmol·mol$^{-1}$ | Eq. 2 | |
| $K_c$ | Michaelis Menten coefficients of Rubisco activity for CO2 | μmol·mol$^{-1}$ | Eq. 6 | |
| $K_o$ | Michaelis Menten coefficients of Rubisco activity for O2 | mmol·mol-1 | Eq. 7 | |
| $O$ | intercellular O2 concentration | mmol·mol-1 | coef | 210 |
| $J_{max}$ | potential maximum rate of electron transport | μmol·m$^{-2}$·s$^{-1}$ | Eq. 4 | |
| $J_{max25}$ | potential maximum rate of electron transport at 25°C | μmol·m$^{-2}$·s$^{-1}$ | cali | 75.56 |
| $J$ | electron transport rate | μmol·m$^{-2}$·s$^{-1}$ | Eq. 3 | |
| $\alpha$ | quantum yield of electron transport | | coef | 0.24 |
| $R$ | gas constant | J·mol-1·K-1 | coef | 8.314 |
| $\Delta S$ | entropy term | J·mol-1·K-1 | coef | 629.26 for $V_{cmax}$<br>631.88 for $J_{max}$ |
| $E_a$ | rate of exponential increase of the biochemical parameters below the optimum temperature | J·mol-1 | coef | 58550 for $V_{cmax}$<br>29680 for $J_{max}$ |
| $H_d$ | rate of decrease of the biochemical parameters above the optimum temperature | J·mol-1 | coef | 200,000 |
| $g_m$ | mesophyll conductance | mol·m$^{-2}$·s$^{-1}$ | | infinity |
| $c_c$ | CO2 concentration in the carboxylation site of chloroplast thylakoids | μmol·mol$^{-1}$ | | $c_i$ |
| $A_c$ | simulated net photosynthetic rate under Rubisco limitation | μmol·m-2·s-1 | Eq. 9 | |
| $A_j$ | simulated net photosynthetic rate under RuBP limitation | μmol·m-2·s-1 | Eq. 9 | |
| $\lambda$ | marginal water cost for unit carbon assimilation | mol·mol-1 | Eq. 13 | |

'meas' in source column indicates that the parameter was measured using a photosynthetic system; 'cali' indicates that the parameter was calibrated by $A$-$c_i$ curves; 'coef' indicates that the parameter was a preset coefficient; the 'Eq." indicates that the parameter was calculated using the corresponding equation.

approximated by the intercellular $CO_2$ concentration ($c_i$) (Equation 8):

$$g_m = \frac{A}{c_i - c_c}, \quad g_m \to \infty, \ c_i = c_c \tag{8}$$

By substituting Equations 2, 3 into Equation 1, the simulated net photosynthetic rates under Rubisco limitation ($A_c$) and RuBP limitation ($A_j$) can be calculated, and the lower one was taken as the net photosynthesis rate. The photosynthetic characteristic parameters $K_m$, $\Gamma^*$, $V_{cmax25}$, $J_{max25}$, and $R_{d25}$ were fitted from $A$-$c_i$ response curve data using Equation 9, and the calibrated results are shown in Figure 3.

$$\begin{cases} A_c = \frac{V_{cmax} c_i}{c_i + K_m}\left(1 - \frac{\Gamma^*}{c_i}\right) - R_d \\ A_j = \frac{\alpha Q (c_i - \Gamma^*)}{(4c_i + 8\Gamma^*)\left(1 + \frac{\alpha^2 Q^2}{J_{max}^2}\right)^{0.5}} - R_d \end{cases} \tag{9}$$

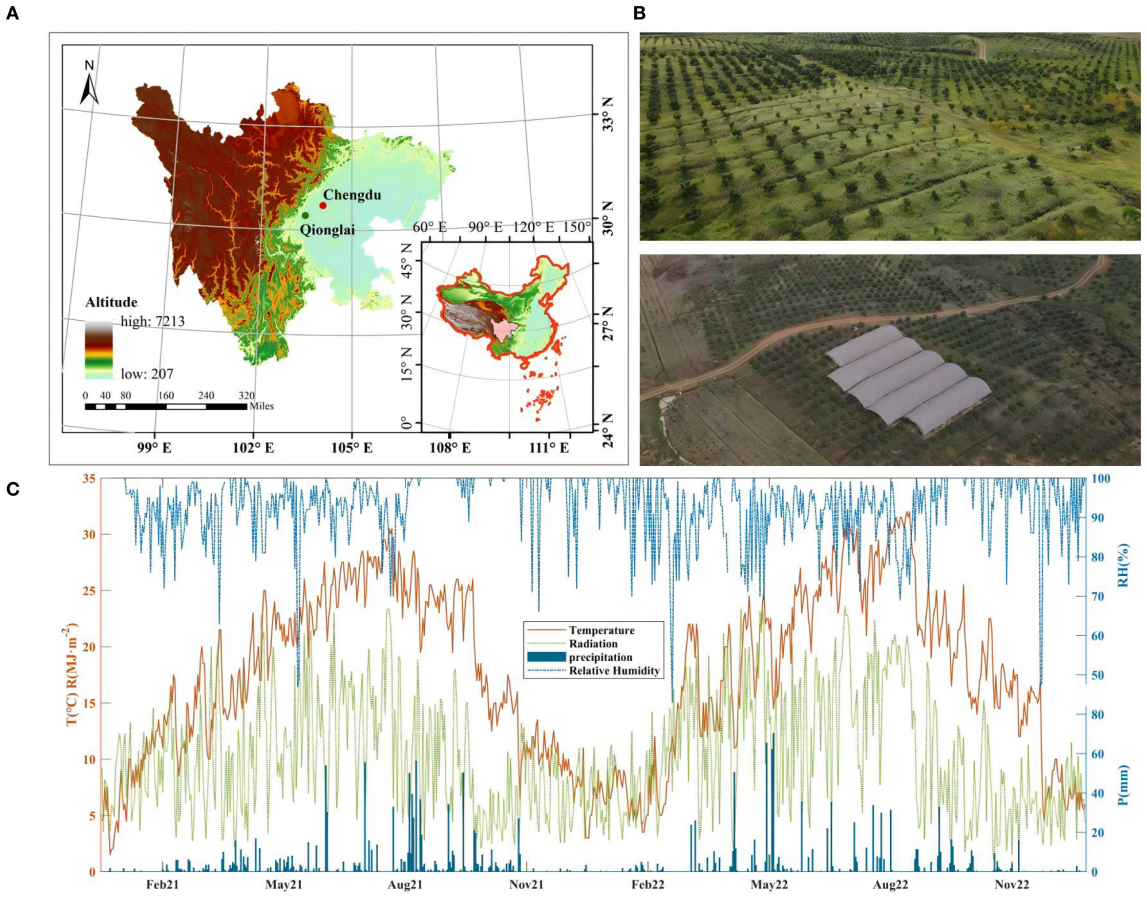


FIGURE 1
Geographic location and climatic condition of experimental site.

### 2.3.2 Calculation of the marginal water cost of carbon gain

The initial expression for the marginal water cost per unit carbon assimilation ($\lambda$) is given by Equation 10:

$$\lambda = \frac{\partial E / \partial g_s}{\partial A / \partial g_s} \times 10^3 \tag{10}$$

Where $A$ is the net carbon assimilation rate, μmol·m$^{-2}$·s$^{-1}$; $E$ is the water transpiration rate, mmol·m$^{-2}$·s$^{-1}$; $g_s$ is the stomatal conductance, mol·m$^{-2}$·s$^{-1}$; a factor of $10^3$ is applied for unit consistency.

Assuming that mesophyll and boundary conductances are large enough to have a negligible impact, $\lambda$ can be calculated using Equation 11 (Buckley et al., 2017):

$$\lambda = \frac{E\left(\frac{1.6}{g_s} + \frac{1}{\partial A / \partial C_i}\right)}{\frac{1.6}{g_s} A} \tag{11}$$

Based on the FvCB functions (Equation 9), $\partial A/\partial c_i$ can be obtained as the partial derivative of $A$ with respect to $c_i$. Consequently, $\lambda$ can be calculated by Equations 12, 13:

$$\frac{\partial A_c}{\partial C_i} = \frac{V_{cmax}(K_m + \Gamma^*)}{(C_i + K_m)^2}, \quad \frac{\partial A_j}{\partial C_i} = \frac{3J\Gamma^*}{4(C_i + 2\Gamma^*)^2} \tag{12}$$

$$\begin{cases} \lambda = \frac{E}{A}\left(1 + \frac{g_s(c_i + K_m)^2}{1.6V_{cmax}(K_m + \Gamma^*)}\right), & A_c < A_j \\ \lambda = \frac{E}{A}\left(1 + \frac{g_s(c_i + 2\Gamma^*)^2(1 + \frac{\alpha^2 Q^2}{J_{max}^2})^{0.5}}{1.2\alpha Q\Gamma^*}\right), & A_j < A_c \end{cases} \tag{13}$$

### 2.3.3 Establishment of the $g_s$-$E$-$A$ coupled optimal stomatal conductance-based models

The coupled optimal stomatal conductance-based models (OSCMs) are constructed by integrating three components: Fick's gas diffusion law (Equation 14), the FvCB biochemical model (Equation 9), and the constant-$\lambda$ optimal stomatal regulation hypothesis (Equation 15). The OSCMs can solve $A$, $c_i$, $E$, and $g_s$ simultaneously. The original equations are as follows:

$$\begin{cases} E = g_s \frac{D}{P} \\ A = \frac{1}{1.6} g_s (c_a - c_i) \end{cases} \tag{14}$$

$$\lambda = \text{constant} \tag{15}$$


FIGURE 2
Leaf gas exchange measurements using a portable photosynthesis system.

Where $P$ is the atmospheric pressure at the leaf surface, kPa.

The final formulas derived for Rubisco limitation (OSCvc model) are given in Equation 16:

$$\begin{cases} \frac{\lambda P}{1.6D} = \frac{1}{(c_a - c_i)} + \frac{\left(\frac{c_i + K_m}{c_a - c_i}\right)^2 \left(\frac{V_{cmax}(c_i - \Gamma^*)}{c_i + K_m} - R_d\right)}{V_{cmax}(K_m + \Gamma^*)} \\ A = \frac{V_{cmax}(c_i - \Gamma^*)}{c_i + K_m} - R_d \\ g_s = \max\left\{\frac{1.6}{(c_a - c_i)} A,\ g_{min}\right\} \\ E = g_s \frac{D}{P} \end{cases} \quad (16)$$

The final formulas derived for RuBP limitation (OSCvj model) are given in Equation 17:

$$\begin{cases} \frac{\lambda P}{1.6D} = \frac{1}{(c_a - c_i)} + \frac{1.6\left(\frac{c_i + 2\Gamma^*}{c_a - c_i}\right)^2 \left(\frac{\alpha Q\left(c_i - \Gamma^*\right)}{4\left(c_i + 2\Gamma^*\right)} - R_d\left(1 + \frac{\alpha^2 Q^2}{J_{max}^2}\right)^{0.5}\right)}{1.2\alpha Q\Gamma^*} \\ A = \frac{\alpha Q\left(c_i - \Gamma^*\right)}{4\left(c_i + 2\Gamma^*\right)\left(1 + \frac{\alpha^2 Q^2}{J_{max}^2}\right)^{0.5}} - R_d \\ g_s = \max\left\{\frac{1.6}{(c_a - c_i)} A,\ g_{min}\right\} \\ E = g_s \frac{D}{P} \end{cases} \quad (17)$$

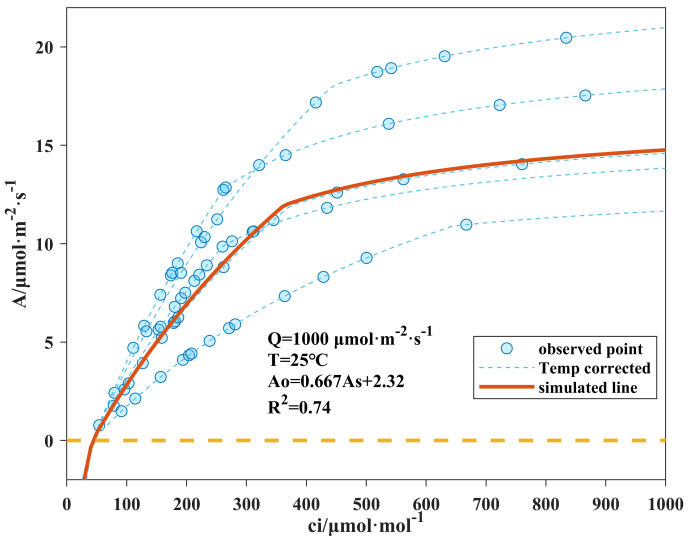


FIGURE 3
Fitted *A-ci* response curves. Points on the dashed lines are single-leaf measurements and corrected to 25 °C5 Solid lines are model simulations based on the average coefficients calibrated from the five measurement curves. $A_o$ denotes the temperature-corrected observation leaf photosynthesis rate; $A_s$ denotes the modeled rate calculated from the averaged coefficients at corresponding intercellular $CO_2$ concentrations.

The coupled optimal stomatal conductance-based models (OSCMs) are established as Equations 16, 17, corresponding to the OSCvc and OSCvj forms. In these models, once $c_i$ is determined from the topmost expression, it can be used in the subsequent equations to solve for $A$, $g_s$, and $E$. To prevent negative simulated values of $g_s$, a minimum stomata conductance ($g_{min}$) of 0.01 mol·m$^{-2}$·s$^{-1}$ is imposed in this study.

The specific implementation steps of OSCMs are as follows: 1) Determining the photosynthesis characteristics parameters $V_{cmax25}$, $J_{max25}$, and $R_{d25}$ from $A$-$c_i$ curves and applying temperature correction; 2) Calculating the marginal water cost of carbon gain $\lambda$ and determining a representative constant value; 3) Using OSCvc or OSCvj model to solve foliar gas exchange parameters including $c_i$, $A$, $E$, and $g_s$.

In steps 1–2, the characteristic coefficients are derived from surveyed gas exchange data, and can also be obtained from published studies on related species. In step 3, only $c_a$, $P$, and $D$, are direct inputs for the OSCvc model (with $Q$ added for the OSCvj model), while $T_l$ or $T_a$ is also necessary to adjust $K_m$, $\Gamma^*$, $V_{cmax}$, $J_{max}$, and $R_d$ to actual temperature. Finally, based on the OSCMs, foliar gas exchange ($A$, $E$, $c_i$, $g_s$) can be simulated using species-specific parameters ($V_{cmax25}$, $J_{max25}$, $R_{d25}$, $\lambda$) and meteorological inputs ($c_a$, $P$, $D$, $Q$, $T_a$).

## 2.4 Analysis

### 2.4.1 Analysis of parameter correlations

A structural equation model (SEM) incorporating meteorological parameters ($c_a$, $D$, $Q$, $T_a$), leaf gas exchange parameters ($A$, $E$, $c_i$, $g_s$), and the marginal water cost of carbon gain ($\lambda$) was established using SPSS Amos 28 (IBM Inc., Armonk, USA) to analyze the relationships between meteorological parameters and foliar gas exchange.

### 2.4.2 Model evaluation

The performance of the OSCMs models is evaluated by four indicators (Equations 18–21). The determination coefficient ($R^2$) indicates the goodness of model fit, while the mean absolute error (MAE), relative mean bias error (MBE) and absolute relative error (RE) reflect model accuracy in terms of magnitude and proportion.

$$R^2 = \frac{(\sum_{i=1}^{n}(O_i - \bar{O})(P_i - \bar{P}))^2}{\sum_{i=1}^{n}(O_i - \bar{O})^2 \sum_{i=1}^{n}(P_i - \bar{P})^2}, \quad (18)$$

$$MAE = \frac{1}{n}\sum_{i=1}^{n}|P_i - O_i| \quad (19)$$

$$MBE = \frac{\sum_{i=1}^{n}(P_i - O_i)}{\sum_{i=1}^{n}O_i} \quad (20)$$

$$|RE|_i = \frac{|P_i - O_i|}{O_i} \quad (21)$$

Where $P_i$ is the predicted value of gas exchange indicators, and $O_i$ is the corresponding observed value; $\bar{P}$ and $\bar{O}$ are the mean values of predicted and observed datasets, respectively. Model performance improves as MAE, MBE, and RE decrease and $R^2$ approaches 1.

### 2.4.3 Model sensitivity

The model sensitivity coefficient quantifies the response of the model to variations in each input variable or parameter. A reference state was defined as an observed gas exchange data point under moderate meteorological conditions ($T_a$ = 35°C, $D$ = 2.0 kPa). The sensitivity coefficient (SC) was then calculated from OSC model simulations with perturbed inputs using Equations 22, 23:

$$SC_i = \frac{(S_i - S)/S}{(F_i - F)/F} \quad (22)$$

$$SC = \frac{\sum_{i=1}^{n}SC_i}{n} \quad (23)$$

Where S is the observed gas exchange value at the reference state, including $g_s$, $c_i$, $A$, and $E$; $S_i$ is the corresponding simulated value with adjusted inputs; F is the observed value of a model factor at the reference state, including $P$, $D$, $c_a$, $Q$, $T_a$, $\lambda$, $V_{cmax25}$, $J_{max25}$, and $R_{d25}$; $F_i$ is the corresponding adjusted value, with only one factor varied at a time; i is the adjustment level, i=1–8, corresponding to -20%, -15%, -10%, -5%, 5%, 10%, 15% and 20%; n is the number of adjustment levels, with n=8 in this study.

# 3 Results

## 3.1 Diurnal variability and representative values of $\lambda$

The numerical solutions of the marginal water cost of carbon gain ($\lambda$) within the 10–90% range for each measurement day, are shown in Figures 4A–C for all points, $V_c$-limited, and $V_j$-limited points, respectively. Values of $\lambda$ exhibited diurnal variability with an average coefficient of variance (CV) of 55.0%, and the fluctuation expanded to 74.6% and 65.7% under $V_c$, and $V_j$ limitations, respectively. Despite this variability, the median $\lambda$ values for individual testing days were relatively stable. For the co-limited dataset, median $\lambda$ ranged in 520.89–3135.39. The distribution range shifted to 360.87–3134.98 under $V_c$ limitation and 594.94–3248.67 under $V_j$ limitation. Since the $\lambda$ values across different days were distributed within comparable ranges, diurnal variability was not explicitly considered, and the median value was adopted as the citrus characteristic value for subsequent simulations. Accordingly, $\lambda$ was set to 1787.10, 1478.51, and 2703.65 under co-limited, $V_c$-limited, and $V_j$-limited conditions, respectively, reflecting differences in leaf carbon-water trade-offs under contrasting photosynthesis limitations.

To further explore the drivers of $\lambda$ variability, a structural equation model (SEM) was constructed based on ambient meteorological variables, leaf gas exchange variables, and $\lambda$ (Figure 4D). The environmental component (green blocks) comprised photosynthetic photon flux density ($Q$), air temperature ($T_a$), vapor pressure deficit ($D$), and ambient $CO_2$ concentration ($c_a$). Among these, $Q$, $T_a$, and $c_a$ were determined as

10.3389/fpls.2026.1748139

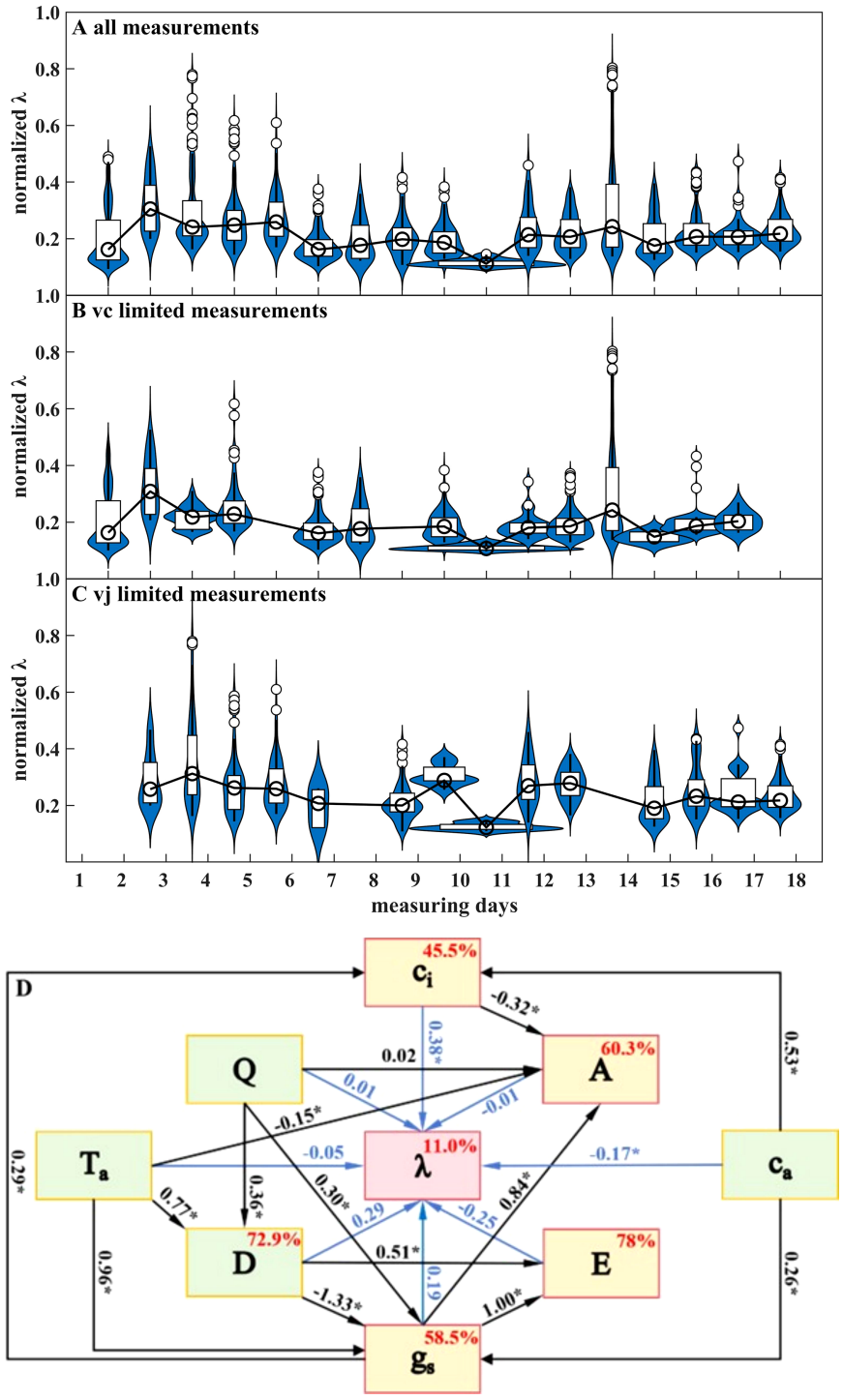


FIGURE 4
**(A–C)** Violin plots of normalized $\lambda$ values across different measurement days under co-limited, $V_c$-limited, and $V_j$-limited conditions; **(D)** Standardized structural equation model (SEM) linking meteorological factors, leaf gas exchange variables, and $\lambda$. Values in boxes indicate the explained variance, and numbers along the arrows represent standardized path coefficients. One standard deviation change in a source variable results in a corresponding deviation in the target variable. Asterisks indicate that the regression weight is significant at the 0.001 level. Standardized path coefficients exceeding 1 reflect the tight coupling among vapor pressure deficit, stomatal conductance, and transpiration, rather than model misspecification.

independent variables, whereas $D$ was modeled as jointly driven by $Q$ and $T_a$. The leaf component (yellow blocks) included net carbon assimilation rate ($A$), transpiration rate ($E$), intercellular $CO_2$ concentration ($c_i$), and stomatal conductance ($g_s$). $A$ and $E$ were assumed to affect gas exchange indirectly through stomatal regulation, rather than exerting direct effects on each other. As a connected bridge, $g_s$ was affected by all environmental variables and, in turn, influenced all leaf gaseous exchange parameters. Based on this SEM, the combined explanatory rate of all eight indicators for $\lambda$ only reached 11%. Among all meteorological factors, only $c_a$ exerted

significant influence on $\lambda$, with a direct effect of -0.17 and an indirect effect of 0.25 through $c_i$ and $g_s$. Among all variables, *Q*, *Ta*, and *ci* showed positive effects on $\lambda$, whereas E had a negative effect, and the remaining variables contributed negligibly (total effects<0.01). Meteorological and gas exchange variables were not the intrinsic drivers for $\lambda$ variability.

## 3.2 Performances of the OSCMs

The simulation results of citrus leaf gas exchange parameters are presented in Figure 5. In the OSCvc and OSCvcd models, photosynthesis was assumed to be limited solely by Rubisco carboxylation rate and was calculated using Equation 16 (Figures 5Ba, b); in the OSCvj and OSCvjd models, photosynthesis was limited by RuBP recycle rate and calculated using Equation 17 (Figures 5Bc, d); in the OSC and OSCd models, photosynthetic limitations were distinguished by the method described in 2.3.1 (Figures 5Be, f). The specific $\lambda$ values are shown in Table 3. The OSC, OSCvc, and OSCvj models employed the median $\lambda$ values of the entire phenological period, whereas the OSCd, OSCvcd, and OSCvjd models used daily median $\lambda$ values for each testing day.

For all four gas exchange parameters, models using daily $\lambda$ outperformed those using long-term $\lambda$, highlighting the importance of the main parameter $\lambda$. For $c_i$ simulation, all models achieved high $R^2$ of 0.70–0.81 (Figure 5A). For *A* and $g_s$, the OSCvjd model performed best with $R^2$ values of 0.58 and 0.73, respectively. Without daily $\lambda$ inputs, the OSC model provided the best *A* estimation with an $R^2$ of 0.48 (Figure 5Be). In contrast, *E* estimation showed much lower accuracy with a maximum $R^2$ of only 0.30 achieved by the OSCvjd model (Figure 5Dd).

The $R^2$, MAE, and MBE values of OSCvc, OSCvcd, OSCvj, OSCvjd, OSC, and OSCd models are shown in Figure 6. In both solution schemes of the OSCMs formulations (Equations 16, 17), $c_i$ is calculated first and the OSCvc model got the highest accuracy with $R^2$ of 0.81 and 0.80, MAE of 18.9 and 20.5 $\mu mol \cdot mol^{-1}$ under long-term and daily $\lambda$ inputs, respectively. The OSCvj and OSC models also performed well with $R^2$ of 0.70–0.81, MAE of 21.4–25.5 $\mu mol \cdot mol^{-1}$. All six OSCMs showed a slight overestimation tendency with MBE values of 3.7–6.3%.

In the second step of the coupled equations, *A* is calculated from $c_i$ using the Farquhar functions. Although the OSCvj model performed poorly in $c_i$ estimation, it obtained the highest $R^2$ of 0.42–0.58 for *A* estimation without evident bias. The OSC model also showed acceptable $R^2$ of 0.48–0.54 but exhibited a clear underestimation tendency with MBE values of -26.0–38.2%. In contrast, the OSCvc model showed the lowest accuracy with $R^2$ of 0.32–0.36 and MAE of 2.87–2.99 $\mu mol \cdot m^{-2} \cdot s^{-1}$. These errors may stem from the inapplicability of the temperature correction coefficients (Equations 4–7), variability in photosynthetic characteristic parameters (Table 4), and the neglect of mesophyll resistance (Equation 8).

In the final step, $g_s$ and *E* were calculated by *A* and $c_i$ based on Fick's law of gas diffusion. For $g_s$ simulation, the OSCvjd model achieved the highest accuracy ($R^2$ = 0.73, MBE=-9.3%). The OSCd model also showed good fit accuracy ($R^2$ = 0.63) but exhibited clear underestimation (MBE = -22.0%). All OSCMs performed poorly in *E* simulation ($R^2 \leq 0.30$), showing pronounced underestimation trend with MBE of -10.0–31.6%. Estimation accuracy of all six OSCMs generally declined from $c_i$ to *A*, $g_s$, and *E*, likely due to error propagation among the coupled gas exchange parameters.

Overall, the OSCvj and OSC methods exhibited acceptable performance in simulating citrus leaf $c_i$, *A*, $g_s$, and *E*. With long-term $\lambda$ input, the OSC model outperformed the OSCvj model in $c_i$ and *A* estimation, whereas with daily $\lambda$ input, the OSCvjd model performed best across all four gaseous exchange parameters. The superior performance of the OSC formulation for *A* supports the view that biochemical limitations shift over time, whereas the relatively better performance of the OSCvj formulation for $g_s$ and *E* suggests that light-limitation may be prevalent during our measurements.

## 3.3 Model error and sensitivity analysis of the OSC model

The OSC model was selected for further error analysis as it performed better with long-term $\lambda$ input, which was easier to obtain. The absolute relative errors (|RE|) of $g_s$ simulated the OSC model under varying environmental $T_a$, *Q*, and *D* conditions are shown in Figure 7. Data points with acceptable error (|RE |< 60%) were mainly distributed under moderated meteorological condition, characterized by relatively low $T_a$ and *D*. The best-performing estimates (green points, |RE|< 20%) were primarily found at $T_a$ of 30–40 °C and *D* of 1–2 kPa. Within this range, the mean |RE| and RE were 35.20% and -11.68%, respectively. When $T_a$ exceeded 40 °C or *D* was higher than 5 kPa, |RE| increased sharply reaching 71.17%. In contrast, no clear threshold was observed for *Q*.

The sensitivity coefficients (SC) of the four gas exchange parameters ($c_i$, *A*, $g_s$, and *E*) estimated by the $V_c$-limited and $V_j$-limited OSC models (Equations 16, 17) in response to meteorological inputs (*P*, *D*, $c_a$, *Q*, and $T_a$) and calibrated inputs ($\lambda$, $V_{cmax25}$, $J_{max25}$, and $R_{d25}$) are shown in Figure 8. For $c_i$ simulation (Figures 8Aa, Ba), $c_a$ was the dominant factor in both OSC formulations, while photosynthesis capacity parameters ($V_{cmax25}$, $J_{max25}$, and $R_{d25}$) were negligible effects. For the other three gas exchange parameters, $T_a$ was the most influential factor with the SCs ranging from -2.05 to -2.60 under $V_c$ limitation and from -2.21 to -3.67 under $V_j$ limitation. This may be because $T_a$ affects both leaf biochemical processes and stomatal regulation. In addition, the reference point was set near 35°C (Equation 22), a condition close to optimal for OSC simulation (Figures 7B, C), making deviations caused by $T_a$ fluctuations more pronounced.

Among the calibrated inputs, $V_{cmax25}$, $J_{max25}$, and $R_{d25}$ were used in the Farquhar biochemical model, while $\lambda$ was defined by the optimal stomatal regulation theory. $V_{cmax25}$ had no effect on the $V_j$-limited OSC model since the model (Equation 17) is independent of it. Similarly, $J_{max25}$ did not affect the $V_c$-limited OSC model. The $V_c$-limited OSC model was more sensitive to $V_{cmax25}$ (SC= -0.94) than to $R_{d25}$ (SC = -0.33), whereas the $V_j$-limited OSC model was more sensitive to $R_{d25}$ (SC= -0.52) than to $J_{max25}$ (SC = 0.31). In addition to the photosynthesis capacity parameters, $\lambda$ also influenced OSC model performance, while its sensitivity was smaller (average 0.40 and 0.34 under $V_c$ and $V_j$ limitation, respectively). Notably, the sensitivity of $g_s$ and *E* to $\lambda$ (average 0.58 and 0.57) was higher than that of $c_i$ and *A* (average 0.14 and 0.19).

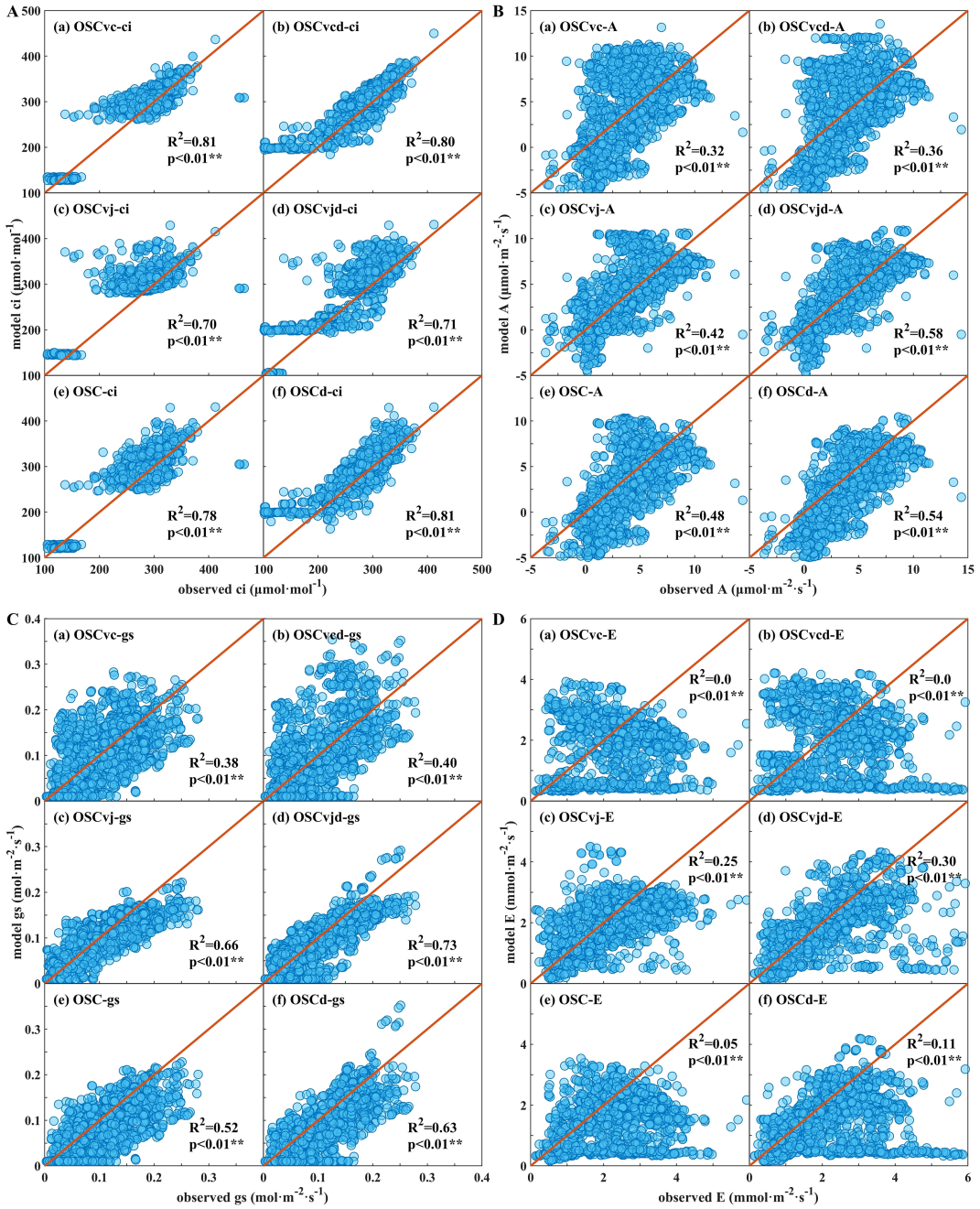


FIGURE 5
**(A)** Intercellular $CO_2$ concentration ($c_i$) simulated by OSCMs; **(B)** Net carbon assimilated rate ($A$) simulated by OSCMs; **(C)** Stomatal conductance ($g_s$) simulated by OSCMs; **(D)** Transpiration rate ($E$) simulated by OSCMs. For the initial OSC, OSCvc, and OSCvj models, $\lambda$ was set as the median value over the entire growth period, whereas for models with subscript "d", $\lambda$ represented the daily median for each testing day.

# 4 Discussion

## 4.1 Meteorological interactions and controls on gas exchange

The climate factors monitored in this study include leaf-surrounding atmospheric temperature, radiation, vapor pressure deficit, and $CO_2$ concentration ($T_a$, $Q$, $vpd$, $c_a$). Among those meteorological factors, only $c_a$ showed significant effect on $\lambda$ (Figure 4d). However, $c_a$ varies little over short periods and is often treated as a background value, so its influence on stomatal regulation is typically neglected. Over broader spatial and temporal scales, its impact would likely be more pronounced, particularly in the context of ongoing greenhouse (Frank et al., 2015; Kirschbaum, 2004).

For the other three factors, $D$ is primarily controlled by $T_a$ and $Q$ with an explanation rate of 72.9% (Figure 4d). In this study, measurements were conducted only on rainless days to avoid equipment damage. Under such conditions, atmospheric water vapor mainly originates from latent heat evaporation driven by radiation and temperature. By definition, $D$ is the ratio of the atmospheric water vapor concentration to the saturation water

10.3389/fpls.2026.1748139

TABLE 3 Diurnal representative values of λ across different measurement days.

| Order | Date (yyyy-mm-dd) | Median value of λ | Median value of λ under vc limited | Median value of λ under vj limited |
|---|---|---|---|---|
| 1 | 2021-04-29 | 520.89 | 525.86 | – |
| 2 | 2021-06-29 | 1,643.41 | 1,667.70 | 1,321.57 |
| 3 | 2021-07-02 | 2,138.93 | 1,780.99 | 3,248.67 |
| 4 | 2021-07-03 | 2,570.25 | 2,240.79 | 2,802.25 |
| 5 | 2021-07-20 | 2,922.37 | – | 2,922.37 |
| 6 | 2021-07-31 | 1,215.57 | 1,191.83 | 1,954.64 |
| 7 | 2021-08-02 | 1,458.09 | 1,458.09 | – |
| 8 | 2021-08-06 | 1,810.29 | – | 1,840.31 |
| 9 | 2021-09-15 | 1,625.71 | 1,599.26 | 3,208.17 |
| 10 | 2022-04-29 | 426.87 | 360.87 | 594.94 |
| 11 | 2022-06-24 | 2,029.29 | 1,511.00 | 2,888.72 |
| 12 | 2022-07-06 | 2,000.97 | 1,696.35 | 3,033.92 |
| 13 | 2022-07-07 | 3,135.39 | 3,134.98 | – |
| 14 | 2022-07-21 | 1,769.87 | 1,228.22 | 2,072.09 |
| 15 | 2022-07-22 | 2,443.56 | 2,032.39 | 2,958.37 |
| 16 | 2022-08-09 | 2,448.98 | 2,378.56 | 2,548.55 |
| 17 | 2022-10-01 | 2,689.75 | – | 2,691.51 |
| median | | 1,787.10 | 1,478.51 | 2,703.65 |

vapor concentration at a given air temperature, and is therefore largely determined by $T_a$ and $Q$ on rainless days.

The thermocouple measuring $T_a$ is positioned very close to the leaf surface, so $T_a$ is influenced by both solar heating and cooling from leaf transpiration. As shown in Figure 7c, $T_a$ initially increases with $Q$, but rises little once $T_a$ reaches around 40 °C. Thus, $T_a$ and $Q$ are the two most dominant and relatively independent meteorological factors affecting foliar gas exchange.

In addition to heating the underlying surface, solar radiation directly supplies energy for plant photosynthesis. Fluctuations in natural light intensity are common (Vialet et al., 2017a), and photosynthetic limitations can shift even over short timescales (Figures 4b, c). Under low irradiance, insufficient photic capture limits the electron transport rate ($V_j$), thereby restricting photosynthesis. As $Q$ increases, sufficient photons drive light reactions, and photosynthesis becomes limited by the availability of reaction substrate, 3-phosphoglycerate (PGA) produced via RuBP carboxylation. Consequently, under high irradiance, the Rubisco carboxylation capacity ($V_c$) becomes the primary limitation to photosynthesis (Liu and van Iersel, 2021; Ye et al., 2021). These shifts highlight the necessity of incorporating dynamic environmental conditions into gas exchange modeling.

## 4.2 Explanations of λ variance

The fundamental principle of optimal stomatal regulation theory is the trade-off between the benefits and costs of stomatal opening. The steady-λ hypothesis adopted in this study focuses on the foliar water-carbon exchange, defining transpired water loss as the cost and photosynthetic carbon assimilation as the benefit (Cowan and Farquhar, 1977). Although most calculated λ points fall within the range of thousands and cluster around the median value with small fluctuations, a few value points rise sharply even exceeding 10,000 (Figure 4). Several possible explanations for this phenomenon are proposed as follows: 1) The λ calculated using Equation 13 would change abruptly when photosynthetic limitation

TABLE 4 The calibrated photosynthesis characteristics parameters derived from the FvCB model.

| Order<br>units | $T_l$<br>°C | $K_m$<br>μmol ·m$^{-2}$·s$^{-1}$ | Γ*<br>μmol ·mol$^{-1}$ | $V_{cmax25}$<br>μmol ·m$^{-2}$·s$^{-1}$ | $J_{max25}$<br>μmol ·m$^{-2}$·s$^{-1}$ | $R_{d25}$<br>μmol ·m$^{-2}$·s$^{-1}$ |
|---|---|---|---|---|---|---|
| 1 | 31.06 | 1,173.59 | 54.60 | 39.09 | 68.87 | 1.45 |
| 2 | 33.13 | 1,406.20 | 60.43 | 56.58 | 86.11 | 2.58 |
| 3 | 29.18 | 1,000.11 | 50.21 | 24.53 | 54.20 | 1.72 |
| 4 | 36.69 | 1,911.34 | 71.66 | 43.98 | 65.02 | 2.30 |
| 5 | 27.81 | 885.32 | 46.47 | 51.85 | 103.61 | 0.81 |
| average | | | | 43.21 | 75.56 | 1.77 |

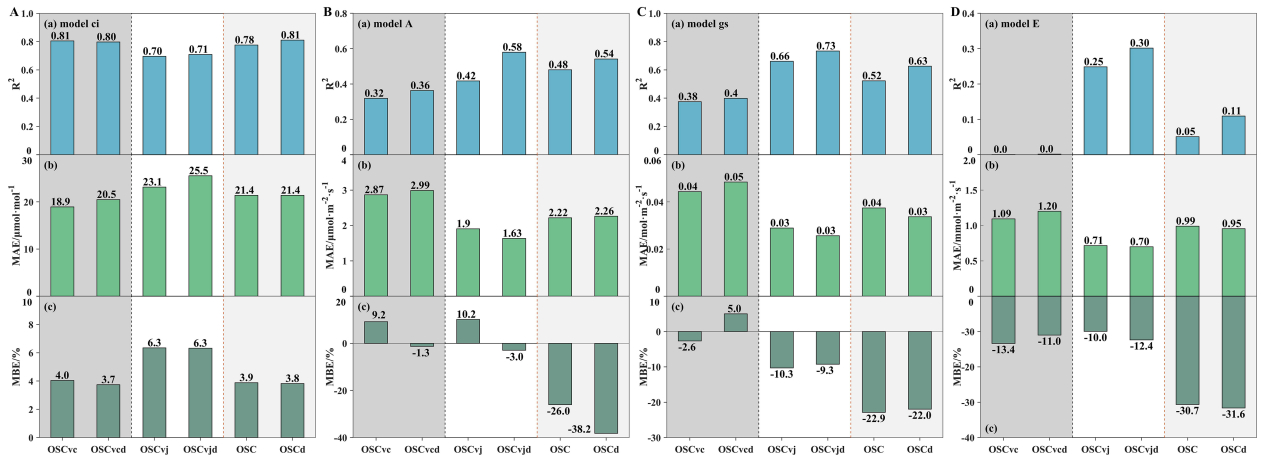


FIGURE 6
**(A)** Coefficient of determination ($R^2$), mean average error (MAE), and relative mean bias error (MBE) of OSCMs for $c_i$ simulation; **(B)** Model performance for $A$ simulation; **(C)** Model performance for $g_s$ simulation; **(D)** Model performance for $E$ simulation.

shift between $V_c$ and $V_j$. Plant physiological parameters that may affect $\lambda$, such as hydraulic conductivity, were not considered (Eller et al., 2020; Manzoni et al., 2011; Sperry et al., 2016). 2) The estimates of $\lambda$ may be biased because mesophyll resistance was negligible, an assumption that is often unrealistic (Flexas et al., 2008; Wistuba et al., 2008). In addition, photosynthetic capacities can vary dynamically (Dewar et al., 2018), and parameters calibrated from limited $A$-$c_i$ curves without strict environmental control may not be universally applicable. 3) If the ability to maintain a relatively stable $\lambda$ is considered an indicator of stomatal regulation capacity, this capacity may be compromised under extreme environmental stress, leading to abrupt increase in $\lambda$ (Mäkelä et al., 2002).

Similar variability in $\lambda$ have also been observed under large shifts in atmospheric $CO_2$, temperature, and vapor pressure deficit (Huang et al., 2021; Katul et al., 2010; Thomas et al., 1999). Fundamentally, these explanations are consistent in that water use in optimality theory should not only be represented solely by instantaneous leaf transpiration but also account for long-term hydraulic safety and whole-plant development.

The discrepancy between realistic $\lambda$ and the constant $\lambda$ used in the OSCMs highlights their inherent limitations. Especially at high $T_a$ and $D$ conditions, large deviations may occur even under sufficient irrigation (60–75% $\theta_f$). To improve the accuracy of gas exchange simulations, additional constraints such as plant hydraulic safety, leaf water potential, and legacy effects should also be incorporated into the optimization framework (Dewar et al., 2018; Eller et al., 2020; Feng et al., 2022). Conversely, detecting such $\lambda$ fluctuations may provide useful diagnostic information on plant status from gas exchange measurements. Overall, elucidating stomatal structural evolution, regulatory capacity, and optimization strategies under complex natural conditions remains a long-term challenge (Mäkelä et al., 2002). Further investigation will advance understanding of plant growth and stress resistance across species.

## 4.3 Application of the OSCMs

Errors in the OSCMs mainly originate from mismatches between prescribed parameters and their true physiological values (e.g., $V_{cmax}$, $J_{max}$, $K_m$, $\Gamma^*$, $R_d$, $g_m$, and $\lambda$). Among these parameters, $\lambda$ is particularly problematic. Its calculation (Equation 13) is derived solely from gas exchange relationships without explicitly accounting for water availability. Consequently, the computed values should be interpreted as expected $\lambda$ values during stomatal regulation, rather than the true shadow price of water. For example, $\lambda$ estimated under

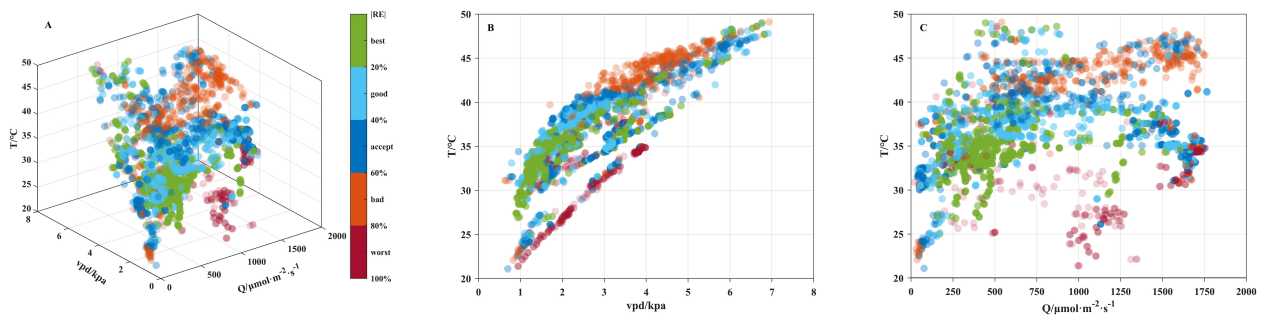


FIGURE 7
**(A)** Absolute relative error (|RE|) of $g_s$ simulated by the OSC model under varying $T$, $Q$, and $D$ conditions; **(B)** |RE| of $g_s$ simulated the OSC model under varying $T$ and $D$ conditions; **(C)** |RE| of $g_s$ simulated the OSC model under varying $T$ and $Q$ conditions.

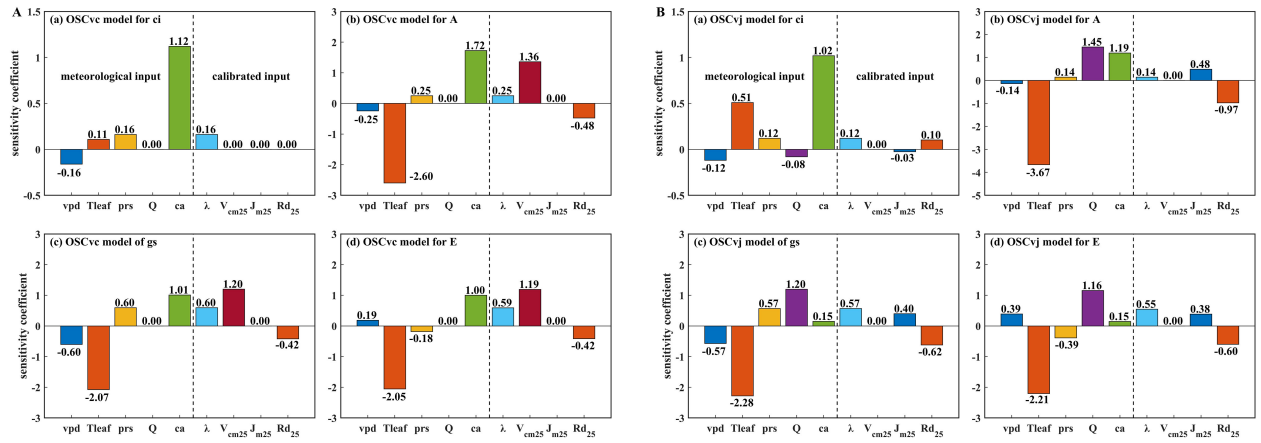


FIGURE 8
**(A)** Sensitivity coefficients of gas exchange variables ($c_i$, $A$, $g_s$, and $E$) simulated by $V_c$-limited OSC model in response to meteorological inputs ($D$, $T_a$, $P$, $Q$, and $c_a$) and calibrated parameters ($\lambda$, $V_{cmax25}$, $J_{max25}$, and $R_{d25}$); **(B)** Sensitivity coefficients of gas exchange variables simulated by $V_j$-limited OSC model in response to model inputs.

$V_j$ limitation was generally higher than that under $V_c$ limitation (Table 3). Under $V_c$ limitation, $A$ is primarily constrained by $c_i$. Stomatal opening can therefore provide substantial carbon gain relative to water loss, leading the optimization equation to compute a low $\lambda$ (a low apparent cost of stomata opening). In reality, $V_c$ limitation often arise from stomatal closure under water deficit, where the true $\lambda$ should be high because water is more expensive. The inconsistency between expected and actual $\lambda$ helps explain the poor performance of the OSCvc and OSCvcd models. In contrast, under $V_j$ limitation, $A$ is primarily $Q$-limited because favorable plant water status allows stomata to remain open and maintain sufficient $c_i$. Accordingly, the expected $\lambda$ more closely reflects the real trade-off between stomatal opening benefit and water loss, resulting in better performance of the OSCvj and OSCvjd models.

Additionally, as discussed in 4.2, $\lambda$ was assumed to be constant, whereas in reality it varies over time. Therefore, OSCMs using daily $\lambda$ inputs generally performed better than those using long-term $\lambda$ inputs (Figures 5, 6). Moderate environmental conditions without soil or atmospheric drought are therefore recommended, as actual $\lambda$ values are more likely to match the prescribed inputs. As shown in Figure 7c, errors in $g_s$ estimation by the OSC model increased rapidly when $T_a$ exceeded 40°C, indicating a breakdown of the optimal regulation assumptions and model validity. In this study, the OSC model performed best under conditions where $T_a$ and $D$ ranged from 30–40°C and 1–2 kPa, respectively.

Although simplifying trait parameters as constants inevitably introduces errors, this approach remains feasible under limited input conditions. The required observational inputs are even fewer than those of single $g_s$ or $E$ simulation models (Wang et al., 2013). Incorporating additional constraints into the optimization framework or adopting short-term analytic solutions for $\lambda$ would improve its estimation accuracy and overall model performance. Further development of the OSCMs may proceed along two main directions. First, deeper mechanistic understanding and mathematical decomposition of optimal stomatal regulation are needed. Such approaches inevitably demands higher data requirements including root zone moisture, xylem vulnerability, mesophyll conductance, plant hydraulic flow, leaf water potential, and carbon allocation patterns (Dewar et al., 2018; Liang et al., 2018; Mencuccini et al., 2019; Wolf et al., 2016). Second, accounting for temporal lags in stomatal responses and explicitly incorporating them into model applications is essential, particularly under highly fluctuating natural environmental conditions (Holtzman et al., 2024; Vialet et al., 2017b). Beyond further refinement of the OSCMs, addressing the limitations of currently available field-scale meteorological observations calls for complementary strategies. Further research on the feedback of vegetation transpiration on near-surface temperature would simplify plant-scale observations and improve simulations of surface vegetation gas exchange under reduced input requirements. Constructing iterative algorithms based on the energy balance among incoming radiation, latent heat, and sensible heat provides an effective mechanistic approach (Wu et al., 2019).

## 5 Conclusions

This study applied optimal stomatal regulation theory with a constant marginal water-carbon conversion assumption on an artificial citrus orchard in a seasonal arid region of southwestern China. Photosynthetic limitations varied with environmental conditions, and characteristic $\lambda$ values were identified as 1787.10, 1478.51, and 2703.65 for co-limited, $V_c$-limited, and $V_j$-limited conditions, respectively. The OSC-based models (OSCMs) achieved acceptable simulation performance across gas exchange variables, with the OSCvc model providing the highest accuracy for ci ($R^2$ = 0.81), the OSCvj model performing best for $g_s$ and $E$ ($R^2$ = 0.66 and 0.25, respectively), and the co-limited OSC model yielding the highest accuracy for $A$ ($R^2$ = 0.48). Among these formulations, the OSC model showed comparatively stable performance across multiple variables, highlighting its robustness for integrated gas exchange simulations. This work applies optimal stomatal regulation in gas

exchange simulation and offers implications for irrigation management and climate resilience in subtropical orchards.

## Data availability statement

The original contributions presented in the study are included in the article/supplementary material. Further inquiries can be directed to the corresponding authors.

## Author contributions

MF: Investigation, Writing – review & editing, Writing – original draft. ZW: Conceptualization, Funding acquisition, Writing – review & editing. XJ: Funding acquisition, Writing – review & editing, Methodology. NC: Validation, Investigation, Funding acquisition, Writing – review & editing. JZ: Writing – review & editing. SJ: Investigation, Data curation, Writing – review & editing. GZ: Investigation, Writing – review & editing, Data curation. LX: Data curation, Writing – review & editing, Funding acquisition, Project administration. XZ: Data curation, Funding acquisition, Writing – review & editing.

## Funding

The author(s) declared that financial support was received for this work and/or its publication. This study was supported by the National Natural Science Foundation of China (52279041, 52309050), Sichuan Science and Technology Program (2022YFN0021, 2023YFN0024, 2024ZHCG0101, 2024YFHZ0200, 2024YFHZ0217), Shandong Provincial Natural Science Fund of China (ZR2022ME033).

## Conflict of interest

The author(s) declared that this work was conducted in the absence of any commercial or financial relationships that could be construed as a potential conflict of interest.

## Generative AI statement

The author(s) declared that generative AI was not used in the creation of this manuscript.

Any alternative text (alt text) provided alongside figures in this article has been generated by Frontiers with the support of artificial intelligence and reasonable efforts have been made to ensure accuracy, including review by the authors wherever possible. If you identify any issues, please contact us.

## Publisher's note



## References

Abdulbaki, A. S., Alsamadany, H., Alzahrani, Y., and Olayinka, B. U. (2022). Rubisco and abiotic stresses in plants: Current assessment. *Turk. J. Bot.* 46, 541–552. doi: 10.55730/1300-008X.2730

Ball, J. T., Woodrow,, and Berry, J. A. (1987). A Model Predicting Stomatal Conductance and its Contribution to the Control of Photosynthesis under Different Environmental Conditions. *InBiggins,J.(eds) Progress in Photosynthesis Research.* 9Dordrecht: Springer). doi: 10.1007/978-94-017-0519-6_48

Buckley, T. N. (2005). The control of stomata by water balance. *New Phytol.* 168, 275–292. doi: 10.1111/j.1469-8137.2005.01543.x

Buckley, T. N., and Mott, K. A. (2013). Modelling stomatal conductance in response to environmental factors. *Plant Cell Environ.* 36, 1691–1699. doi: 10.1111/pce.12140

Buckley, T. N., Mott, K. A., and Farquhar, G. D. (2003). A hydromechanical and biochemical model of stomatal conductance 26, 1767–1785. doi: 10.1046/j.1365-3040.2003.01094.x

Buckley, T. N., Sack, L., and Farquhar, G. D. (2017). Optimal plant water economy. *Plant Cell Environ.* 40, 881–896. doi: 10.1111/pce.12823

Cowan, I. R., and Farquhar, G. D. (1977). Stomatal function in relation to leaf metabolism and environment. *Symp. Soc Exp. Biol.* 31, 471–505. Available online at: https://www.researchgate.net/publication/22384954.

Delwiche, M. J., and Cooke, J. R. (1977). An analytical model of the hydraulic aspects of stomatal dynamics. *J. Theor. Biol.* 69, 113–141. doi: 10.1016/0022-5193(77)90391-5

Dewar, R., Mauranen, A., Makela, A., Holtta, T., Medlyn, B., Vesala, T., et al. (2018). New insights into the covariation of stomatal, mesophyll and hydraulic conductances from optimization models incorporating nonstomatal limitations to photosynthesis. *New Phytol.* 217, 571–585. doi: 10.1111/nph.14848

Dong, Y., Qi, C., Gu, Y., Gui, C., and Fang, G. (2024). Citrus industry agglomeration and citrus green total factor productivity in China: an empirical analysis utilizing a dynamic spatial durbin model. *Agriculture* 14, 2059. doi: 10.3390/agriculture14112059

Duursma, R. A. (2015). Plantecophys–an R package for analysing and modelling leaf gas exchange data. *PloS One* 10, e0143346. doi: 10.1371/journal.pone.0143346

Eller, C. B., Rowland, L., Mencuccini, M., Rosas, T., Williams, K., Harper, A., et al. (2020). Stomatal optimization based on xylem hydraulics (SOX) improves land surface model simulation of vegetation responses to climate. *New Phytol.* 226, 1622–1637. doi: 10.1111/nph.16419

FAOSTAT (2025). *Food and agricultural organization of united nations* (Rome). Available online at: https://www.fao.org/faostat/es/data (accessed.

Farquhar, G. D., von Caemmerer, S., and Berry, J. A. (1980). A biochemical model of photosynthetic CO2 assimilation in leaves of C3 species. *Planta* 149, 78–90. doi: 10.1007/BF00386231

Feng, X., Lu, Y., Jiang, M., Katul, G., Manzoni, S., Mrad, A., et al. (2022). Instantaneous stomatal optimization results in suboptimal carbon gain due to legacy effects. *Plant Cell Environ.* 45, 3189–3204. doi: 10.1111/pce.14427

Flexas, J., Ribas-Carbo, M., Diaz-Espejo, A., Galmes, J., and Medrano, H. (2008). Mesophyll conductance to CO2: current knowledge and future prospects. *Plant Cell Environ.* 31, 602–621. doi: 10.1111/j.1365-3040.2007.01757.x

Frank, D. C., Poulter, B., Saurer, M., Esper, J., Huntingford, C., Helle, G., et al. (2015). Water-use efficiency and transpiration across European forests during the Anthropocene. *Nat. Clim. Change* 5, 579–583. doi: 10.1038/nclimate2614

Hetherington, A. M., and Woodward, F. I. (2003). The role of stomata in sensing and driving environmental change. *Nature* 424, 901–908. doi: 10.1038/nature01843

Holtzman, N., Sloan, B., Potkay, A., Katul, G., Feng, X., Konings, A. G., et al. (2024). Ecosystem water-saving timescale varies spatially with typical drydown length. *AGU Adv.* 5. doi: 10.1029/2023AV001113

Huang, G., Yang, Y., Zhu, L., Peng, S., and Li, Y. (2021). Temperature responses of photosynthesis and stomatal conductance in rice and wheat plants. *Agric. For. Meteorol* 300, 108322. doi: 10.1016/j.agrformet.2021.108322

Jarvis and, P., and G.J.P.T.o.t.R.S.o.L (1976). The interpretation of the variations in leaf water potential and stomatal conductance found in canopies in the field. *J Philosophical Transactions of the Royal Society of London* 273, 593–610. doi: 10.1098/rstb.1976.0035

Ji, S., Tong, L., Kang, S., Li, F., Lu, H., Du, T., et al. (2017). A modified optimal stomatal conductance model under water-stressed condition. *Int. J. Plant Prod.* 11, 295–314.

Katul, G., Manzoni, S., Palmroth, S., and Oren, R. (2010). A stomatal optimization theory to describe the effects of atmospheric CO2 on leaf photosynthesis and transpiration. *Ann. Bot.* 105, 431–442. doi: 10.1093/aob/mcp292

Kirschbaum, M. U. (2004). Direct and indirect climate change effects on photosynthesis and transpiration. *Plant Biol. (Stuttg.)* 6, 242–253. doi: 10.1055/s-2004-820883

Knauer, J., Zaehle, S., Medlyn, B. E., Reichstein, M., Williams, C. A., Migliavacca, M., et al. (2018). Towards physiologically meaningful water-use efficiency estimates from eddy covariance data. *Glob Chang Biol.* 24, 694–710. doi: 10.1111/gcb.13893

Liang, Y., Gao, Y., Wang, G., Si, Z., Shen, X., Duan, A., et al. (2018). Luxury transpiration of winter wheat and its responses to deficit irrigation in North China Plain. *Plant Soil Environ.* 64, 361–366. doi: 10.17221/331/2018-PSE

Lin, Y. S., Medlyn, B. E., Duursma, R. A., Prentice, I. C., Wang, H., Baig, S., et al. (2015). Optimal stomatal behaviour around the world. *Nat. Clim. Change* 5, 459–464. doi: 10.1038/nclimate2550

Liu, C., Wang, Q., Makela, A., Hokka, H., Peltoniemi, M., Holtta, T., et al. (2022). A model bridging waterlogging, stomatal behavior and water use in trees in drained peatland. *Tree Physiol.* 42, 1736–1749. doi: 10.1093/treephys/tpac037

Liu, J., and van Iersel, M. W. (2021). Photosynthetic physiology of blue, green, and red light: light intensity effects and underlying mechanisms. *Front. Plant Sci.* 12, 619987. doi: 10.3389/fpls.2021.619987

Lu, Y., Duursma, R. A., and Medlyn, B. E. (2016). Optimal stomatal behaviour under stochastic rainfall. *J. Theor. Biol.* 394, 160–171. doi: 10.1016/j.jtbi.2016.01.003

Mäkelä, A., Givnish, T. J., Berninger, F., Buckley, T. N., Farquhar, G. D., Hari, P., et al. (2002). Challenges and opportunities of the optimality approach in plant ecology. *SilvaFennica* 36, 605–614. doi: 10.14214/sf.528

Manzoni, S., Vico, G., Katul, G., Fay, P. A., Polley, W., Palmroth, S., et al. (2011). Optimizing stomatal conductance for maximum carbon gain under water stress: a meta-analysis across plant functional types and climates. *Funct. Ecol.* 25, 456–467. doi: 10.1111/j.1365-2435.2010.01822.x

Manzoni, S., Vico, G., Palmroth, S., Porporato, A., and Katul, G. (2013). Optimization of stomatal conductance for maximum carbon gain under dynamic soil moisture. *Adv. Water Resour.* 62, 90–105. doi: 10.1016/j.advwatres.2013.09.020

Marchin, R. M., Medlyn, B. E., Tjoelker, M. G., and Ellsworth, D. S. (2023). Decoupling between stomatal conductance and photosynthesis occurs under extreme heat in broadleaf tree species regardless of water access. *Glob Chang Biol.* 29, 6319–6335. doi: 10.1111/gcb.16929

Medlyn, B. E., Duursma, R. A., De Kauwe, M. G., and Prentice, I. C. (2013). The optimal stomatal response to atmospheric CO2 concentration: Alternative solutions, alternative interpretations. *Agric. For. Meteorol.* 182-183, 200–203. doi: 10.1016/j.agrformet.2013.04.019

Medlyn, B. E., Dreyer, E., Ellsworth, D., Forstreuter, M., Harley, P. C., Kirschbaum, M. U. F., et al. (2002). Temperature response of parameters of a biochemically based model of photosynthesis. *II. A Rev. Exp. data. Plant Cell Environ.* 25, 1167–1179. doi: 10.1046/j.1365-3040.2002.00891.x

Medlyn, B. E., et al. (2011). Reconciling the optimal and empirical approaches to modelling stomatal conductance. *Global Change Biol.* 17, 2134–2144. doi: 10.1111/j.1365-2486.2010.02375.x

Mencuccini, M., Manzoni, S., and Christoffersen, B. (2019). Modelling water fluxes in plants: from tissues to biosphere. *New Phytol.* 222, 1207–1222. doi: 10.1111/nph.15681

Mrad, A., Sevanto, S., Domec, J. C., Liu, Y., Nakad, M., Katul, G., et al. (2019). A dynamic optimality principle for water use strategies explains isohydric to anisohydric plant responses to drought. *Front. For. Global Change* 2. doi: 10.3389/ffgc.2019.00049

Munjonji, L., Ayisi, K. K., Mafeo, T. P., Maphanga, T., and Mabitsela, K. E. (2021). Seasonal variation in soil CO2 emission and leaf gas exchange of well-managed commercial Citrus sinensis (L.) orchards. *Plant Soil* 465, 65–81. doi: 10.1007/s11104-021-04986-x

Negi, J., Hashimoto-Sugimoto, M., Kusumi, K., and Iba, K. (2014). New approaches to the biology of stomatal guard cells. *Plant Cell Physiol.* 55, 241–250. doi: 10.1093/pcp/pct145

Palangasinghe, P. C., Liyanage, W. K., Wickramasinghe, M. P., Palangasinghe, H. R., Shih, H. C., Shiao, M. S., et al. (2024). Reviews on Asian citrus species: Exploring traditional uses, biochemistry, conservation, and disease resistance. *Ecol. Genet. Genomics* 32, 100269. doi: 10.1016/j.egg.2024.100269

Perdomo, J. A., Capo-Bauca, S., Carmo-Silva, E., and Galmes, J. (2017). Rubisco and rubisco activase play an important role in the biochemical limitations of photosynthesis in rice, wheat, and maize under high temperature and water deficit. *Front. Plant Sci.* 8, 490. doi: 10.3389/fpls.2017.00490

Potkay, A., Cabon, A., Peters, R. L., Fonti, P., Sapes, G., Sala, A., et al. (2025a). Generalized stomatal optimization of evolutionary fitness proxies for predicting plant gas exchange under drought, heatwaves, and elevated CO2. *Global Change Biol.* 31. doi: 10.1111/gcb.70049

Potkay, A., Sloan, B., and Feng, X. (2025b). Stomatal parameters in a changing environment. *Plant Cell Environ.* 48, 2986–2997. doi: 10.1111/pce.15293

Rogers, A., Kumarathunge, D. P., Lombardozzi, D. L., Medlyn, B. E., Serbin, S. P., Walker, A. P., et al. (2021). Triose phosphate utilization limitation: an unnecessary complexity in terrestrial biosphere model representation of photosynthesis. *New Phytol.* 230, 17–22. doi: 10.1111/nph.17092

Santini, J., Giannettini, J., Pailly, O., Herbette, S., Ollitrault, P., Berti, L., et al. (2012). Comparison of photosynthesis and antioxidant performance of several Citrus and Fortunella species (Rutaceae) under natural chilling stress. *Trees* 27, 71–83. doi: 10.1007/s00468-012-0769-5

Schymanski, S. J., Roderick, M. L., and Sivapalan, M. (2015). Using an optimality model to understand medium and long-term responses of vegetation water use to elevated atmospheric CO2 concentrations. *AoB Plants* 7, plv060. doi: 10.1093/aobpla/plv060

Sharkey, T. D. (1985). Photosynthesis in intact leaves of C3 plants: Physics, physiology and rate limitations. *Botanical Rev.* 51, 53–105. doi: 10.1007/BF02861058

Souza, G. M., Ribeiro, R. V., and Pincus, S. M. (2004). Changes in network connectance and temporal dynamics of gas exchange in Citrus sinensis under different evaporative demands. *Braz. J. Plant Physiol.* 16, Dec2004. doi: 10.1590/S1677-04202004000300001

Sperry, J. S., Venturas, M. D., Anderegg, W. R. L., Mencuccini, M., Mackay, D. S., Wang, Y., et al. (2016). Predicting stomatal responses to the environment from the optimization of photosynthetic gain and hydraulic cost. *Plant Cell Environ.* 40, 816–830. doi: 10.1111/pce.12852

Thomas, D. S., Eamus, D., and Bell, D. (1999). Optimization theory of stomatal behaviour I. A critical evaluation of five methods of calculation. *J. Exp. Bot.* 332, 385–392. doi: 10.1093/jxb/50.332.385

Tominaga, J., and Kawamitsu, Y. (2024). Combined leaf gas-exchange system for model assessment. *J. Exp. Bot.* 75, 2982–2993. doi: 10.1093/jxb/erae081

Venturas, M. D., Sperry, J. S., Love, D. M., Frehner, E. H., Allred, M. G., Wang, Y., et al. (2018). A stomatal control model based on optimization of carbon gain versus hydraulic risk predicts aspen sapling responses to drought. *New Phytol.* 220, 836–850. doi: 10.1111/nph.15333

Vialet, C. S., Matthews, J. S. A., McAusland, L., Blatt, M. R., Griffiths, H., Lawson, T., et al. (2017b). Temporal dynamics of stomatal behavior: modeling and implications for photosynthesis and water use. *Plant Physiol.* 174, 603–613. doi: 10.1104/pp.17.00125

Vialet, C. S., Matthews, J. S., Simkin, A. J., Raines, C. A., and Lawson, T. (2017a). Importance of fluctuations in light on plant photosynthetic acclimation. *Plant Physiol.* 173, 2163–2179. doi: 10.1104/pp.16.01767

Vico, G., Manzoni, S., Palmroth, S., Weih, M., and Katul, G. (2013). A perspective on optimal leaf stomatal conductance under CO2 and light co-limitations. *Agric. For. Meteorol.* 182-183, 191–199. doi: 10.1016/j.agrformet.2013.07.005

Volpe, V., Manzoni, S., Marani, M., and Katul, G. (2011). Leaf conductance and carbon gain under salt-stressed conditions. *J. Geophys. Res.* 116. doi: 10.1029/2011JG001848

Wang, Y., Sperry, J. S., Venturas, M. D., Trugman, A. T., Love, D. M., Anderegg, W. R. L., et al. (2019). The stomatal response to rising CO2 concentration and drought is predicted by a hydraulic trait-based optimization model. *Tree Physiol.* 39, 1416–1427. doi: 10.1093/treephys/tpz038

Wang, Y., Long, Q., Li, Y., Kang, F., Fan, Z., Xiong, H., et al. (2022). Mitigating magnesium deficiency for sustainable citrus production: A case study in Southwest China. *Sci. Hortic.* 295, 110832. doi: 10.1016/j.scienta.2021.110832

Wang, Y., Sperry, J. S., Anderegg, W. R. L., Venturas, M. D., and Trugman, A. T. (2020). A theoretical and empirical assessment of stomatal optimization modeling. *New Phytol.* 227, 311–325. doi: 10.1111/nph.16572

Wang, C., Yang, P., Li, Y., and Ren, S. (2013). Characteristics of E. japonicus stomatal conductance under water-deficit stress using a nonlinear Jarvis modified model. Math. *Comput. Modell.* 58, 799–806. doi: 10.1016/j.mcm.2012.12.024

Wistuba, N., Reich, R., Wagner, H. J., Zhu, J. J., Schneider, H., Bentrup, F. W., et al. (2008). Xylem flow and its driving forces in a tropical liana: concomitant flow-sensitive NMR imaging and pressure probe measurements. *Plant Biol.* 2, 579–582. doi: 10.1055/s-2000-16644

Wolf, A., Anderegg, W. R., and Pacala, S. W. (2016). Optimal stomatal behavior with competition for water and risk of hydraulic impairment. *Proc. Natl. Acad. Sci. U. S. A.* 113, E7222–E7230. doi: 10.1073/pnas.1615144113

Wu, A., Hammer, G. L., Doherty, A., von Caemmerer, S., and Farquhar, G. D. (2019). Quantifying impacts of enhancing photosynthesis on crop yield. *Nat. Plants* 5, 380–388. doi: 10.1038/s41477-019-0398-8

Ye, Z. P., Duan, S. H., Chen, X. M., Duan, H. L., Gao, C. P., Kang, H. J., et al. (2021). Quantifying light response of photosynthesis: addressing the long-standing limitations of non-rectangular hyperbolic model. *Photosynthetica* 59, 185–191. doi: 10.32615/ps.2021.009